Penerbit Akademia Baru

CFD Letters

Journal homepage: www.akademiabaru.com/cfdl.html
ISSN: 2180-1363

Effect of Buoyancy Force on The Flow and Heat Transfer Around a Thin Needle in Al_2O_3- Cu Hybrid Nanofluid

Open Access

Siti Nur Alwani Salleh[1,*], Norfifah Bachok[1,2], Norihan Md Arifin[1,2], Fadzilah Md Ali[1,2]

[1] Institute for Mathematical Research, Universiti Putra Malaysia, 43400, UPM Serdang, Selangor, Malaysia
[2] Department of Mathematics, Faculty of Science, Universiti Putra Malaysia, 43400, UPM Serdang, Selangor, Malaysia

ARTICLE INFO

Article history:
Received 21 November 2019
Received in revised form 16 January 2020
Accepted 21 January 2020
Available online 29 January 2020

ABSTRACT

An analysis has been performed to study the effect of buoyancy force in the boundary layer flow past a thin needle in a hybrid nanofluid. In this study, we have taken into consideration a combination of two types of nanoparticles which are alumina and copper in the base fluid. The coupled nonlinear partial differential equations representing momentum and heat equations are reduced into a set of nonlinear ordinary differential equations. The transformed equations are evaluated numerically by adopting the bvp4c method with the help of MATLAB software. Effects of involved controlling physical parameters, namely buoyancy or mixed convection parameter, velocity ratio parameter, solid volume fraction parameters and needle thickness on the skin friction coefficient and heat transfer rate as well as velocity and temperature profiles are indicated through graphs and then discussed. It is revealed that the addition of every 0.2% alumina and copper nanoparticle (ϕ_1 and ϕ_2) into a base fluid tends to enhance the heat transfer rate for about 18% up to 44%. It is worth knowing that the existence of dual branches of the solution is noted when the flow is opposing ($\lambda < 0$) and when the needle against the free stream direction ($\varepsilon < 0$).

Keywords:
Thin needle; Buoyancy force; Hybrid nanofluid; Multiple solutions; Stability analysis

1. Introduction

A few decades ago, the existence of nanofluid as a heat transfer fluid becoming one of the subjects of interest in fluid mechanics. This subject is well received by several researchers due to the ordinary fluids are less preferred in the heat transfer process. However, the metallic nanoparticles that contain high thermal conductivity could be an excellent approach if we mixed those nanoparticles into the regular fluids. Choi [1] delivered the brilliant idea of nanofluid by preparing it through an experimental study. Since the nanoliquids tends to enhance the heat transmission process, hence, diverse amount of applications can be traced in industries. By the way of example, manufacturing of paper, heat exchanger, microelectronic devices, nuclear reactors, geothermal power generation and transportations. The related works inspired by this topic were reported in Rana

* *Corresponding author.*
E-mail address: alwani24salleh@gmail.com (Siti Nur Alwani Salleh)

and Bhargava [2], Bachok *et al.,* [3], Salleh *et al.,* [4], Japar *et al.,* [5] and Acharya *et al.,* [6] considering various surfaces and physical effects.

In certain heat transfer applications, the consumption of nanosolution is less prominent. To rectify this deficiency, hybrid nanofluid is created by consolidating two different types of nanoparticles in the regular fluids. Similar to nanofluid with one component or nanoparticle, hybrid or combined nanomaterials have a very small dimension that is 10-100 nm in diameter. In order to form the hybrid nanofluid, nanoparticles with different types: metallic (Ag, Al, Cu and Zn) and non-metallic or metal oxide (Al_2O_3, CuO, MgO and Fe_3O_4) must undergo a synthetization process. A detail and comprehensive study of the process has been analyzed by Sarkar *et al.,* [7]. In their study, they found that the metallic nanomaterials possess high thermal conductivity, but weak in stability and reactivity. Contrary to that, metal oxide has low thermal conductivity, but good in other properties like stability and reactivity. In the present analysis, the hybrid nanosuspension between copper (Cu) and (Al_2O_3) has been given attention. The combination of those nanomaterials would definitely augment the hydrodynamic flow and heat transfer around a thin needle. The effectiveness of hybrid nanofluid compared to ordinary nanofluid and regular fluids in heat transport is certified through many experimentally and theoretically studies [8-12]. Authentically, hybrid nanomaterials have very unusual features that a single component cannot possess. It may be lacking in some of the thermal or chemical properties. Unlike a nanofluid, hybrid nanofluid has many good properties such as better mechanical resistance, chemical stability, thermal conductivity, physical strength and so on [7]. Possible areas in which hybrid nanofluid is widely used include air conditioning systems, solar heating, microfluidics, space aircrafts and ships, vehicle thermal management, medical and lubrication.

The influence of alumina-copper hybrid nanofluid has been discussed by Moghadassi *et al.,* [13], and they noticed that hybrid nanofluid offers a better performance of heat transfer compared to nanofluid. The heat transport analysis of copper-alumina/water hybrid nanofluid on a stretched surface is performed by Devi and Devi [14]. Mehryan *et al.,* [15] examined the flow of natural convection in a cavity filled with a porous medium immersed in a hybrid nanoliquid. Ashorynejad and Shahriari [16] communicated the influence of a magnetic field for hybrid nanofluid in an open wavy cavity. Furthermore, Mansour *et al.,* [17] demonstrated the entropy analysis of heat source and sink on natural convection in a hybrid nanoliquid with a magnetic effect. The problem of the inclined magnetic field over a slippery sheet in hybrid nanofluid has been conducted by Acharya *et al.,* [18]. In the same year, Acharya *et al.,* [19] investigated the consequence of Hall current on hybrid nanosolution past a revolving disk. The comprehensive investigations on the hybrid nanofluid topic are presented in Refs. [20-25].

The flow over a thin needle is a very important and significant process due to it has numerous applications especially in engineering and biomedical areas. It is typically used in circulatory problems, transportations, wire coating and in hot wire anemometer or protected thermocouple for computing the wind velocity. The motion of the needle perturbs the free-stream flow, and this is the main focus of the flow and heat transfer analysis in experimental studies for finding the velocity and temperature profiles. This extraordinary feature of the thin needle makes such a topic interesting for some researchers. Lee [26] started to investigate the boundary layer flow past a stretching surface in a viscous fluid by discussing the asymptotic behaviors of the system. Narain and Uberoi [27] performed the forced convection flow over an isothermal thin needle in a viscous fluid. A year later, Narain and Uberoi [28] examined the mixed convection flow on the slender needle by taking into consideration both isoflux and isothermal wall situations. Subsequently, Chen and Smith [29] studied analytically the steady forced convection flow and heat transfer from the nonisothermal thin needle. More works on the thin needle in a viscous fluid can be found in the current literature [30-32].

The study of a thin needle in a nanofluid is first considered by Grosan and Pop [33]. In their research, they solve the effect of variable wall temperature on the classical problem of forced convection heat transfer past a thin needle. The problem of stagnation point flow in water-carbon nanofluid with variable heat flux on the thin needle is investigated by Hayat *et al.,* [34]. In recent years, many researchers include Ahmad *et al.,* [35], Soid *et al.,* [36], Salleh *et al.,* [37-38] had performed the numerical studies on the thin needle in nanofluid by using various physical effects. Very recently, Salleh *et al.,* [39] carried out a stability analysis of nanofluid flow and heat transfer past a slender needle by considering the heat generation and chemical reaction effects. The consideration of stability analysis has been introduced by Merkin [40] after he got an idea of how to identify the stable solution (or physically realizable) if there exists more than one solution in a system. Since the work of Merkin [40] has been well received, more publications are found in the existing literature [41-44].

Being motivated by the above-referred studies, in this work, we examined the steady behavior of incompressible flow and wall heat transfer on a continuously moving thin needle saturated by hybrid nanofluid in the presence of buoyancy effect. By proposing the hybrid colloidal suspension in the current model, we truly feel that it is capable to assist engineers in designing some applications related to the thermal removal process. The governing mathematical system is computed numerically via MATLAB function bvp4c. Graphical demonstrations have been made for the velocity, temperature, skin friction coefficient and local Nusselt number with respect to some pertinent parameters.

2. Mathematical Analysis

The flow of alumina-copper hybrid nanofluid of uniform ambient temperature T_∞ past a moving thin needle of uniform wall temperature T_w is examined. The flow system is assumed to be in the x direction, which is along the needle surface, and r axis is normal to it as shown in Figure 1. In Figure 1, U_w denotes a uniform velocity of the needle that moves in the same and opposite ways to the free stream flow of uniform velocity U_∞, and $r = R(x)$ represents the needle radius. Taking into account the above considerations, equations for the continuity, momentum and energy can be written as Grosan *et al.,* [33] and Salleh *et al.,* [36]:

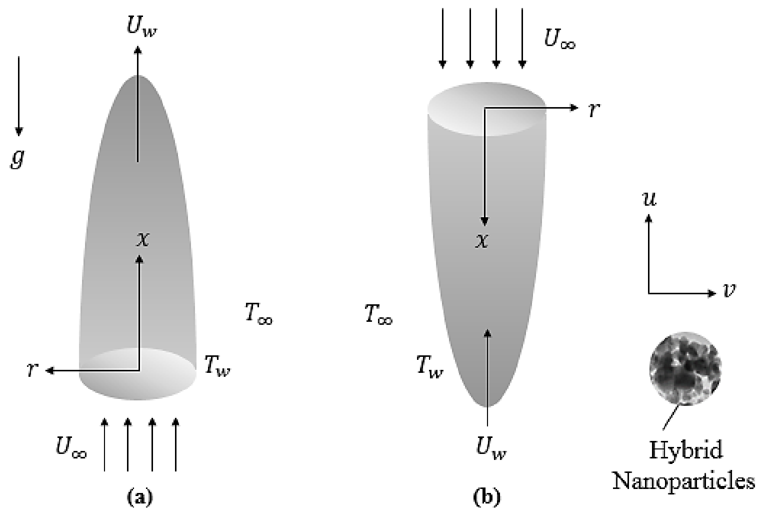

Fig. 1. Cylindrical coordinate system: (a) assisting flow and (b) opposing flow

$$(ru)_x + (rv)_r = 0, \tag{1}$$

$$uu_x + vu_r = \frac{\mu_{hnf}}{\rho_{hnf}} \frac{1}{r} (ru_r)_r + \frac{(\rho\beta)_{hnf}}{\rho_{hnf}} g(T - T_\infty), \tag{2}$$

$$uT_x + vT_r = \frac{1}{r} \frac{k_{hnf}}{(\rho C_p)_{hnf}} (rT_r)_r \tag{3}$$

The corresponding boundary conditions for Eqs. (1) to (3) are

$$\begin{aligned} &u = U_w, \quad v = 0, \quad T = T_w \ \text{ at } \ r = R(x), \\ &u \to U_\infty, \quad T \to T_\infty \ \text{ as } \ r \to \infty, \end{aligned} \tag{4}$$

where the velocities components along x and r axis are u and v, respectively. Besides that, T is the temperature of nanofluid, μ is the dynamic viscosity, ρ is the density, β is the volumetric expansion coefficient, k is the thermal conductivity, g is the acceleration due to gravity and C_p is the specific heat at uniform pressure. The subscripts '*hnf*', '*nf*' and '*s*' represent the terms for 'hybrid nanofluid', 'nanofluid' and 'solid nanoparticle', respectively. The solid nanoparticles volume fraction for alumina and copper are given by ϕ_1 and ϕ_2, respectively.

The thermophysical properties of the base fluid and solid nanoparticles at 25 $\circ C$ and the applied models for physical properties of hybrid nanofluid and nanofluid are tabulated in Table 1 and Table 2, respectively.

Table 1
Thermophysical properties of regular fluid and solid nanoparticles (Oztop and Abu-Nada [45])

Properties	Water	Al_2O_3	Cu
$\beta \times 10$ $(1/K)$	21	0.85	1.67
C_p (J/kg K)	4180	765	385
k (W/mK)	0.6071	40	400
ρ (kg/m)	997.0	3970	8933

The stream function $\psi(x, r)$ defined as $u = r^{-1}\psi_r$ and $v = -r^{-1}\psi_x$ which satisfies the continuity Eq. (1). Next, we introduce the following dimensionless and similarity variables [33,36] into Eqs. (1) to (4)

$$\psi = \nu x f(\eta), \quad \eta = \frac{Ur^2}{\nu x}, \quad \theta(\eta) = \frac{T - T_\infty}{T_w - T_\infty}, \tag{5}$$

in which $\theta(\eta)$ is the dimensionless temperature with η as the similarity variable. Introducing the above transformations (5) into Eqs. (2) to (4), yields the following non-linear equations:

$$\frac{1}{B_1 B_2}(2\eta f''' + 2f'') + ff'' + \frac{B_3}{B_2}\frac{\lambda}{4}\theta = 0, \tag{6}$$

$$\frac{2C_1}{\Pr C_2}(\eta\theta''+\theta')+f\theta'=0. \tag{7}$$

Table 2
Thermophysical properties of nanofluid and hybrid nanofluid (Devi and Devi [14])

Properties	Hybrid Nanofluid	Nanofluid
Dynamic viscosity	$\mu_{hnf}=\frac{\mu_f}{(1-\phi_1)^{2.5}(1-\phi_2)^{2.5}}$	$\mu_{nf}=\frac{\mu_f}{(1-\phi)^{2.5}}$
Buoyancy coefficient	$(\rho\beta)_{hnf}=(1-\phi_2)[(1-\phi_1)(\rho\beta)_f+\phi_1(\rho\beta)_{s_1}]+\phi_2(\rho\beta)_{s_2}$	$(\rho\beta)_{nf}=(1-\phi)(\rho\beta)_f+\phi(\rho\beta)_s$
Density	$\rho_{hnf}=(1-\phi_2)[(1-\phi_1)\rho_f+\phi_1\rho_{s_1}]+\phi_2\rho_{s_2}$	$\rho_{nf}=(1-\phi)\rho_f+\phi\rho_s$
Heat capacity	$(\rho C_p)_{hnf}=(1-\phi_2)\left[(1-\phi_1)(\rho C_p)_f+\phi_1(\rho C_p)_{s_1}\right]+\phi_2(\rho C_p)_{s_2}$	$(\rho C_p)_{nf}=(1-\phi)(\rho C_p)_f+\phi(\rho C_p)_s$
Thermal Conduc-tivity	$\frac{k_{hnf}}{k_{bf}}=\frac{k_{s_2}+2k_{bf}-2\phi_2(k_{bf}-k_{s_2})}{k_{s_2}+2k_{bf}+\phi_2(k_{bf}-k_{s_2})}$, where $\frac{k_{bf}}{k_f}=\frac{k_{s_1}+2k_f-2\phi_1(k_f-k_{s_1})}{k_{s_1}+2k_f+\phi_1(k_f-k_{s_1})}$	$\frac{k_{nf}}{k_f}=\frac{k_s+2k_f-2\phi(k_f-k_s)}{k_s+2k_f+\phi(k_f-k_s)}$

such that

$$B_1=(1-\phi_1)^{2.5}(1-\phi_2)^{2.5},$$
$$B_2=(1-\phi_2)\left[(1-\phi_1)+\phi_1\frac{\rho_{s1}}{\rho_f}\right]+\phi_2\frac{\rho_{s2}}{\rho_f},$$
$$B_3=(1-\phi_2)\left[(1-\phi_1)+\phi_1\frac{(\rho\beta)_{s1}}{(\rho\beta)_f}\right]+\phi_2\frac{(\rho\beta)_{s2}}{(\rho\beta)_f},$$

and

$$C_1=\frac{k_{hnf}}{k_f}=\frac{k_{s2}+2C_0k_f-2\phi_2(C_0k_f-k_{s2})}{k_{s2}+2C_0k_f+\phi_2(C_0k_f-k_{s2})}C_0 \quad \text{where} \quad C_0=\frac{k_{s1}+2k_f-2\phi_1(k_f-k_{s1})}{k_{s1}+2k_f+\phi_1(k_f-k_{s1})},$$
$$C_2=(1-\phi_2)\left[(1-\phi_1)+\phi_1\frac{(\rho C_p)_{s1}}{(\rho C_p)_f}\right]+\phi_2\frac{(\rho C_p)_{s2}}{(\rho C_p)_f}. \tag{8}$$

The transformed boundary conditions are now becoming

$$f(c)=\frac{\varepsilon}{2}c,\quad f'(c)=\frac{\varepsilon}{2},\quad \theta(c)=1,$$
$$f'(\eta)=\frac{1}{2}(1-\varepsilon),\quad \theta(\eta)\to 0 \quad \text{as} \quad \eta\to\infty. \tag{9}$$

Here, primes refer to differentiation with respect to η where $\eta=c$ is the needle thickness, λ is the mixed convection parameter, ε is the velocity ratio or moving parameter between the surface and the flow with the composite velocity of $U=U_w+U_\infty$ and $\Pr$ is the Prandtl number. These parameters and dimensionless numbers are defined as follows:

$$\lambda = \frac{Gr_x}{\mathrm{Re}_x^2}, \quad \varepsilon = \frac{U_w}{U}, \quad \mathrm{Pr} = \frac{\nu}{\alpha} \tag{10}$$

where the local Grashof number is $Gr_x = (T_w - T_\infty) g \beta_f x^3/\nu^2$ and the local Reynolds number is $\mathrm{Re}_x = Ux/\nu$. Noteworthy when $\lambda > 0$, the flow is assisting and when $\lambda < 0$, the flow is opposing.

The practical quantities in this study are the shear stress coefficient or skin friction C_f and the local Nusselt number Nu_x which is defined by

$$C_f = \frac{\mu_{hnf}}{\rho U^2}(u_r)_{r=c} = \frac{4c^{1/2}}{(1-\phi_1)^{2.5}(1-\phi_2)^{2.5}}(\mathrm{Re}_x)^{-1/2} f''(c) \tag{11}$$

$$Nu_x = -\frac{x}{(T_w - T_\infty)}(T_r)_{r=c} = -\frac{2k_{hnf}}{k_f} c^{1/2} (\mathrm{Re}_x)^{1/2} \theta'(c) \tag{12}$$

3. Stability Analysis

To perform a stability analysis, first we consider the unsteady form of Eqs. (2) and (3) as follows:

$$u_t + uu_x + vu_r = \frac{\mu_{hnf}}{\rho_{hnf}} \frac{1}{r}(ru_r)_r + \frac{(\rho\beta)_{hnf}}{\rho_{hnf}} g(T - T_\infty), \tag{13}$$

$$T_t + uT_x + vT_r = \frac{1}{r}\frac{k_{hnf}}{(\rho C_p)_{hnf}}(rT_r)_r. \tag{14}$$

By initiating the dimensionless time variable $\tau = 2Ut/x$, the following new similarity variables are

$$\psi(x,r) = \nu x f(\eta,\tau), \quad \eta = \frac{Ur^2}{\nu x}, \quad \theta(\eta,\tau) = \frac{T - T_\infty}{T_w - T_\infty}, \quad \tau = \frac{2Ut}{x}, \tag{15}$$

It is worth knowing that the function of τ in this analysis is well related to an initial value problem that is consistent with the solution that will be yielded in practice. Using Eq. (15) into Eqs. (13) and (14), we obtain

$$\frac{1}{B_1 B_2}\left[2\eta \frac{\partial^3 f}{\partial \eta^3} + 2\frac{\partial^2 f}{\partial \eta^2}\right] + \frac{B_3}{B_2}\frac{\lambda}{4}\theta - \frac{\partial^2 f}{\partial \eta \partial \tau} + \tau \frac{\partial f}{\partial \eta}\frac{\partial^2 f}{\partial \eta \partial \tau} + f\frac{\partial^2 f}{\partial \eta^2} - \tau \frac{\partial^2 f}{\partial \eta^2}\frac{\partial f}{\partial \tau} = 0, \tag{16}$$

$$\frac{C_1}{\mathrm{Pr}\, C_2}\left[2\eta \frac{\partial^2 \theta}{\partial \eta^2} + 2\frac{\partial \theta}{\partial \eta}\right] - \frac{\partial \theta}{\partial \tau} + \tau \frac{\partial f}{\partial \eta}\frac{\partial \theta}{\partial \tau} + f\frac{\partial \theta}{\partial \eta} - \tau \frac{\partial f}{\partial \tau}\frac{\partial \theta}{\partial \eta} = 0, \tag{17}$$

together with the conditions below:

$$\begin{gathered} f(c,\tau) = \tau \frac{\partial f}{\partial \tau}(c,\tau) + \frac{\varepsilon}{2}c, \quad \frac{\partial f}{\partial \eta}(c,\tau) = \frac{\varepsilon}{2}, \quad \theta(c,\tau) = 1, \\ \frac{\partial f}{\partial \eta}(\eta,\tau) \to \frac{1-\varepsilon}{2}, \quad \theta(\eta,\tau) \to 0 \quad \text{as} \quad \eta \to \infty. \end{gathered} \tag{18}$$

In the work of Weidman *et al.,* [44], they introduced the following two equations to identify the stability of the solution $f = f_0(\eta)$ and $\theta = \theta_0(\eta)$ for Eqs. (16) to (18).

$$f(\eta,\tau) = f_0(\eta) + e^{-\gamma\tau} F(\eta,\tau),$$
$$\theta(\eta,\tau) = \theta_0(\eta) + e^{-\gamma\tau} G(\eta,\tau), \tag{19}$$

Here, γ is the eigenvalue parameter, $F(\eta,\tau)$ is the small relative to $f_0(\eta)$ and $G(\eta,\tau)$ is the small relative to $\theta_0(\eta)$.

Replacing Eq. (19) into Eqs. (16) to (18), the following linear eigenvalue problems can be written as:

$$\frac{2\eta}{B_1 B_2} F_0''' + \frac{2}{B_1 B_2} F_0'' + \frac{B_3}{B_2} \frac{\lambda}{4} G_0 + f_0 F_0'' + F_0 f_0'' + \gamma F_0' = 0 \tag{20}$$

$$\frac{2\eta C_1}{\Pr C_2} G_0'' + \frac{2C_1}{\Pr C_2} G_0' + f_0 G_0' + F_0 \theta_0' + \gamma G_0 = 0 \tag{21}$$

Then, the boundary conditions become

$$F_0(c) = 0, \quad F_0'(c) = 0, \quad G_0(c) = 0$$
$$F_0'(\eta) \to 0, \quad G_0(\eta) \to 0 \quad \text{as} \quad \eta \to \infty \tag{22}$$

The next step to perform this stability is to assume $\tau = 0$ which corresponds to an initial growth or decay of the solution (19). Hence, in the meantime functions $F(\eta,\tau)$ and $G(\eta,\tau)$ can be rewritten as $F_0(\eta)$ and $G_0(\eta)$, respectively. There are two possibilities to relax the boundary conditions whether on $F_0'(\eta)$ or on $G_0(\eta)$ (see Harris *et al.,* [46]). For the current work, we choose to relax the condition on $F_0'(\eta) \to 0$ as $\eta \to \infty$. Thus, we solve the system of Eqs. (20) to (22) together with the condition $F_0''(c) = 1$.

4. Numerical Approach

The coupled nonlinear ordinary differential equations (ODEs) from Eqs. (6) to (7) with the related boundary conditions in Eq. (9) are executed numerically via a very efficient technique, called bvp4c solver through MATLAB software. To acquire the solution, we apply the initial guess at the starting mesh point and then modify the step size to gain a particular certainty. To further use this technique, we have to reconstruct the nonlinear ODEs into first-order ODEs. Now, we subsequently propose the following variables:

$$y_1 = f(\eta), \quad y_2 = f'(\eta), \quad y_3 = f''(\eta),$$

$$y_4 = \theta(\eta), \quad y_5 = \theta'(\eta) \tag{23}$$

Where

$$y_1' = y_2, \quad y_2' = y_3, \quad y_4' = y_5. \tag{24}$$

Following this, the Eqs. (6) to (7) can be substituted by

$$y_3' = -\frac{1}{\eta}\left[y_3 + \frac{B_1 B_2}{2} y_1 y_3 + \frac{B_1 B_3}{8} \lambda y_4\right], \tag{25}$$

$$y_5' = -\frac{1}{\eta}\left[y_5 + \frac{Pr}{2}\frac{C_2}{C_1} y_1 y_5\right], \tag{26}$$

and the indispensable boundary conditions are

$$y_{a_1} - \frac{\varepsilon}{2} c = 0, \quad y_{a_2} - \frac{\varepsilon}{2} = 0, \quad y_{a_4} - 1 = 0,$$

$$y_{b_2} - \frac{1}{2}(1-\varepsilon) = 0, \quad y_{b_4} = 0 \tag{27}$$

From the above equations, a and b are regarded as the situations on the surface, $\eta = c$ and far-field, $\eta = \eta_\infty$, respectively.

Afterward, the numerical findings have been reached by guessing the inputs of unidentified parameters λ, ε, c, ϕ_1 and ϕ_2 that satisfied the condition $f'(\eta) \to \frac{1}{2}(1-\varepsilon)$, $\theta(\eta) \to 0$ as $\eta \to \infty$. The procedure is reiterated until the converged solution meets a tolerance limit of 10^{-6}.

5. Code of Verification

To authenticate the validity of the present work, we have initially matched the values of shear stress $f''(c)$ for some values of c when $\mathrm{Pr} = 1$ with Ishak *et al.,* [30] and Soid *et al.,* [36] as given in Table 3. In this comparison, we consider the situation where the needle moves against the free stream flow, $\varepsilon = -1$ for $\lambda = \phi_1 = \phi_2 = 0$. We observed that the numerical values in Table 3 are in an excellent assurance with the existing publication.

Table 3
Values of shear stress $f''(c)$ for $\lambda = \phi_1 = \phi_2 = 0$

c	Ishak *et al.,* [30]		Soid *et al.,* [36]		Current results	
	Upper branch	Lower branch	Upper branch	Lower branch	Upper branch	Lower branch
0.01	26.6021	2.8031	26.599394	2.805533	26.599394	2.805533
0.1	3.7162	0.3884	3.703713	0.389103	3.703714	0.389113
0.2			2.005424	0.227837	2.005427	0.227839

6. Discussion of Results

The aim of this section is to analyze the variations of solid nanoparticles volume fraction (ϕ_1 and ϕ_2), mixed convection parameter (λ), velocity ratio parameter (ε), thickness of the needle (c) on the dimensionless velocity and temperature profiles, skin friction coefficient and the local Nusselt number or heat transfer rate. To get a clear understanding of a present study, these variations are presented with the help of graphical illustrations as shown in Figure 2 to Figure 11. In certain parameter domain, it is revealed that the dual solutions are likely to exist in such domain. The way we differentiate the dual solutions is by considering the upper branch solution as the solution with higher values of reduced skin friction $f''(c)$ and reduced local Nusselt number $-\theta'(c)$, and lower branch solution as the solution with lesser values of $f''(c)$ and $-\theta'(c)$. Throughout this study, the range of the nanoparticle concentration is considered between 0.4% to 2% (see Kumar *et al.,* [47]).

The variation trends of reduced skin friction coefficient and reduced local Nusselt number as well as, the dimensionless velocity and temperature profiles, are demonstrated in Figure 2 to Figure 5 for several types of fluid, namely regular fluid or water ($\phi_1 = \phi_2 = 0$), alumina nanofluid ($\phi_1 = 0.01, \phi_2 = 0$) and alumina-copper hybrid nanofluid ($\phi_1 = \phi_2 = 0.01$). As illustrated in Figures 2 and 3, the reduced skin friction coefficient and the local Nusselt number are higher for hybrid nanofluid followed by nanofluid and water in a certain domain of λ. This situation takes place due to the decrement of both velocity and thermal boundary layer thicknesses at the wall as can be seen in Figures 4 and 5. The truth is by combining two different kinds of nanoparticles, its physical properties will automatically combine each other, and consequently, provides a good performance on both $f''(c)$ and $-\theta'(c)$. An interesting behavior is found in Figures 2 and 3 where the multiple solutions appear in a certain region of mixed convection parameter, say $\lambda_c < \lambda \leq -0.1$. λ_c is the critical value of parameter λ by which the upper and lower branch solutions connect. In addition, only unique solutions exist for $\lambda > 0$ and no solutions for $\lambda < \lambda_c$.

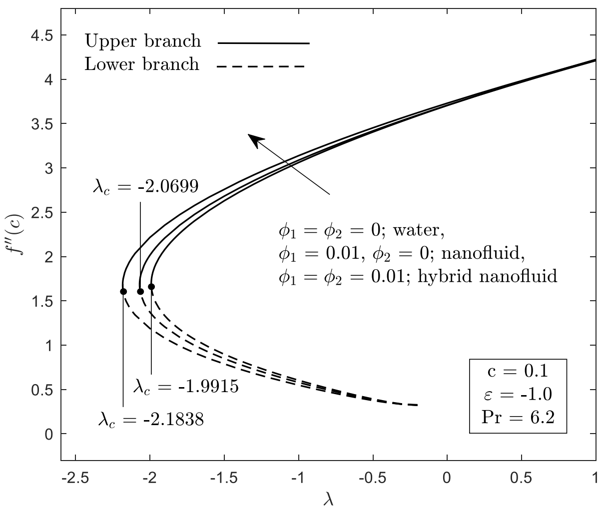

Fig. 2. Variation of ϕ_1 and ϕ_2 on reduced skin friction coefficient $f''(c)$

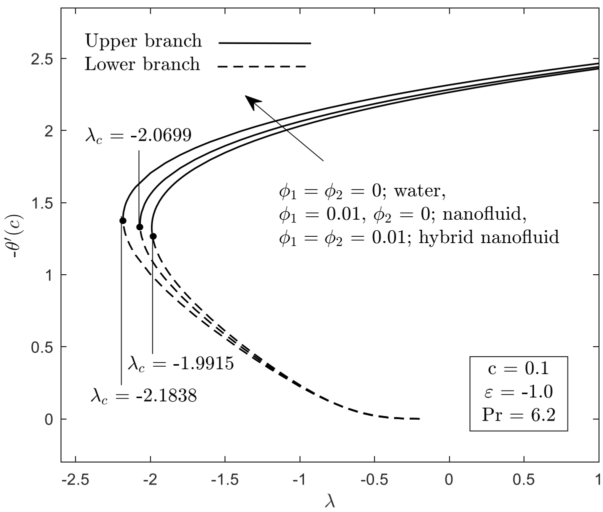

Fig. 3. Variation of ϕ_1 and ϕ_2 on reduced local Nusselt number $-\theta'(c)$

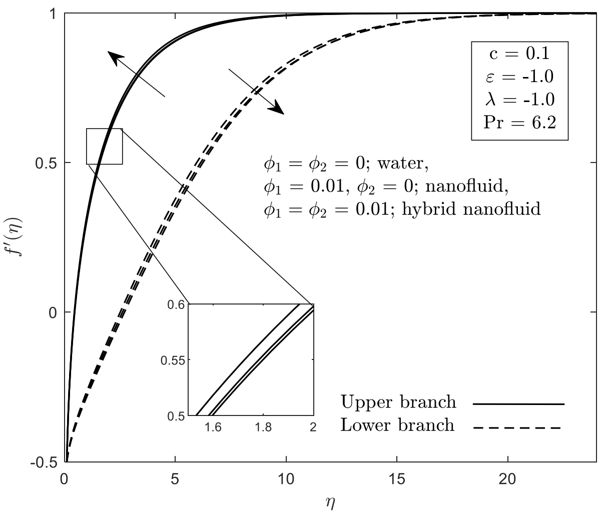

Fig. 4. Variation of ϕ_1 and ϕ_2 on dimensionless velocity profiles $f'(\eta)$

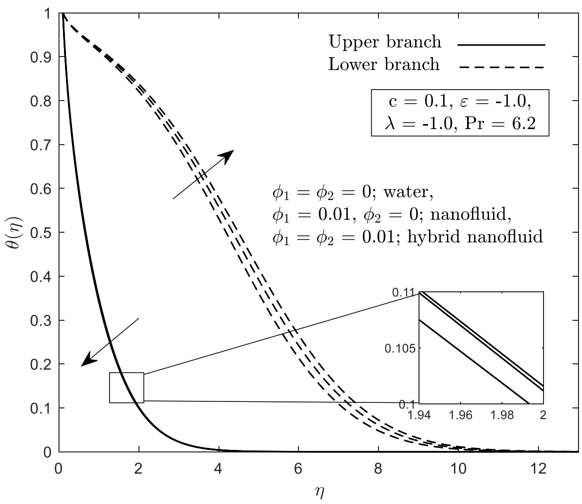

Fig. 5. Variation of ϕ_1 and ϕ_2 on dimensionless temperature profiles $\theta(\eta)$

Figures 6 and 7 illustrated the influence of the copper nanoparticle volume fraction ϕ_2 on reduced skin friction coefficient and reduced local Nusselt number versus velocity ratio parameter ε when $\phi_1 = 0.1$. It is noticed from Figures 6 and 7 that the reduced skin friction coefficient and local Nusselt number enhance with the increase in the parameter ϕ_2. However, the reduced local Nusselt number only augments in a certain range of $-3.06 \le \varepsilon \le -0.3$. The increment in Figure 6 is usually due to the movement of the needle that opposes the direction of free-stream flow ($\varepsilon < 0$) which then causes the velocity ratio to diminish, and as a result, delay the movement of the needle and induces more friction on the surface. Physically, the addition of more copper nanoparticles in the system gives space for drag force to occur on the needle surface. Accordingly, it enhances the magnitude of the reduced skin friction coefficient because of the collision between those nanoparticles. The velocity and temperature distributions for varying copper nanoparticle volume fraction ϕ_2 are presented in Figures 8 and 9. In these profiles, we noted that the monotonic behavior of the lines had satisfied the far-field boundary conditions in Eq. (9). Thus, the numerical result obtained for the current work is confirmed. Besides, the dual solutions are observed to exist when the $\varepsilon_c \le \varepsilon \le -0.1$.

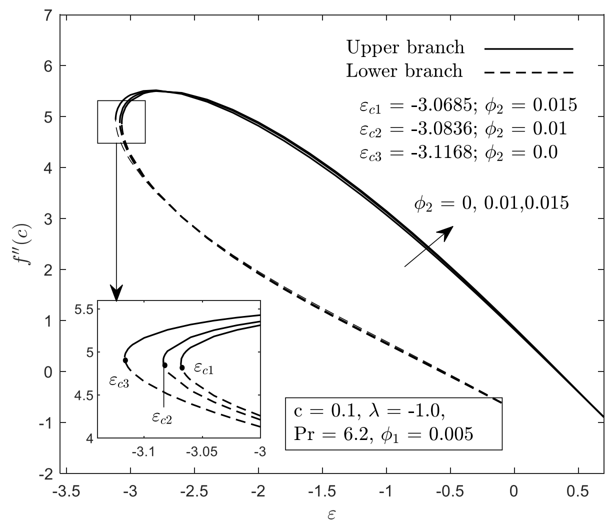

Fig. 6. Variation of ϕ_2 on reduced skin friction coefficient $f''(c)$

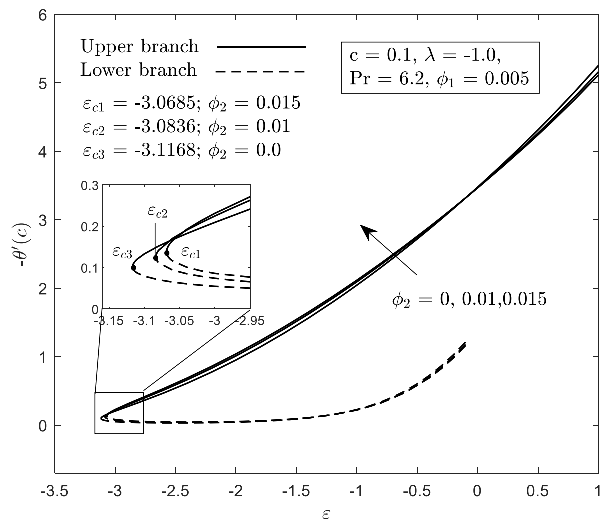

Fig. 7. Variation of ϕ_2 on reduced local Nusselt number $-\theta'(c)$

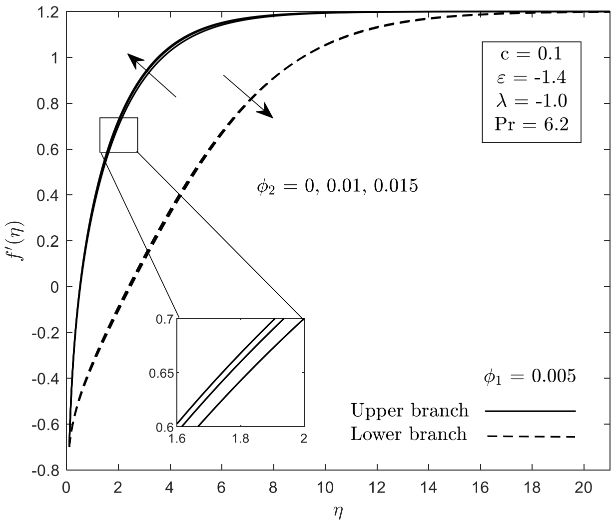

Fig. 8. Variation of ϕ_2 on dimensionless velocity profiles $f'(\eta)$

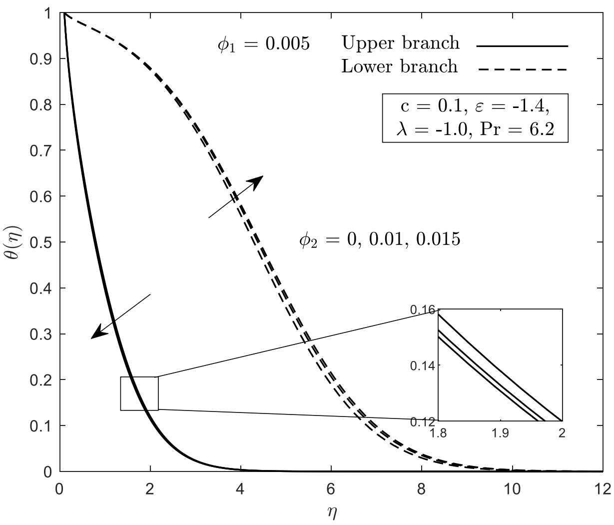

Fig. 9. Variation of ϕ_2 on dimensionless temperature profiles $\theta(\eta)$

Table 4 is prepared to show the effect of the embedded parameters of interest, namely, ϕ_1, ϕ_2, c, λ and ε on the numerical values of the skin friction coefficient and the rate of heat transfer or local Nusselt number when $\Pr = 6.2$. From this table, one can see that the skin friction coefficient $C_f(Re_x)^{1/2}$ and local Nusselt number $Nu_x(Re_x)^{-1/2}$ are noticed to increase as the nanoparticle volume fraction of alumina (ϕ_1) and copper (ϕ_2) increase. When there are many nanoparticles in the flow, it would tend to create more friction on the surface and consequently enhance the skin friction coefficient. In addition, the continuous collision between those nanoparticles helps the heat to quickly transfer from the surface to the fluid. This criterion can increase the rate of heat transfer on the needle surface. From this table, it is observed that the addition of every 0.2% alumina and copper nanoparticle (ϕ_1 and ϕ_2) into a base fluid tends to increase the heat transfer rate for about 18% up to 44%. Besides that, as expected the values of skin friction and heat transfer rate seem to decrease as the needle thicknesses enlarge. This is due to the increment in the momentum and thermal boundary layer thicknesses as the values of c increase as illustrated in Figures 10 and 11. In heat transfer process, the thin wall of the needle reduces the time required for the heat to transfer from the wall to the fluid. This consequently increases the heat transfer rate on the wall. An increase in the values of mixed convection parameter λ increases the skin friction coefficient and heat transfer rate. Meanwhile, the results are invertible as the velocity ratio parameter ε increase.

For the stability analysis results, we present the minimum eigenvalues γ for different values of solid nanoparticle volume fractions (ϕ_1 and ϕ_2) and mixed convection parameter λ as tabulated in Table 5. It is seen from the table that, the upper branch solutions give positive values, whereas the lower branch solutions give negative values. This implies that the upper branch solution is stable and physically realistic, while the lower branch solution is not. Physically, it makes sense because the upper branch solution always takes the highest values which are near to the needle wall. It is worth knowing that the solutions near to the surface always provides a good physical interpretation.

Table 4
Computational values of skin friction coefficient $C_f(Re_x)^{1/2}$ and local Nusselt number $Nu_x(Re_x)^{-1/2}$ for some values of ϕ_1, ϕ_2, c, λ and ε when $\Pr = 6.2$

ϕ_1	ϕ_2	c	λ	ε	$f''(c)$	$C_f(Re_x)^{1/2}$	$-\theta'(c)$	$Nu_x(Re_x)^{-1/2}$
0.0	0.0	0.1	-1.4	-1.6	3.733250	8.249395	1.161716	1.280124
0.01	0.01				3.888061	8.591482	1.298285	1.430613
0.006					3.864804	10.035391	1.276357	1.603928
0.008					3.876544	11.960783	1.287391	1.844254
0.01	0.004				3.838716	6.318874	1.254145	1.044669
	0.006				3.855691	10.011728	1.269169	1.597825
	0.008				3.872130	11.947164	1.283877	1.846356
	0.01	0.08			5.055410	9.991631	1.914767	1.887179
		0.12			3.018988	7.307806	0.862406	1.041009
		0.14			2.125605	5.557527	0.451796	0.589058
		0.1	-1.2		4.091900	9.041907	1.370752	1.510466
			-1.0		4.272328	9.440600	1.432256	1.578239
			-0.8		4.436460	9.803284	1.48621	1.637692
			-1.4	-1.4	3.570228	7.889163	1.519392	1.674256
				-1.2	3.220411	7.116170	1.751543	1.930069
				-1.0	2.843003	6.282208	1.994709	2.198020

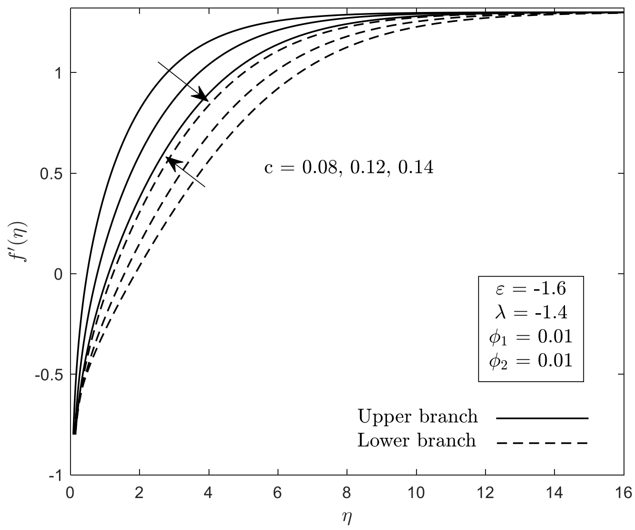

Fig. 10. Variation of c on dimensionless velocity profiles $f'(\eta)$

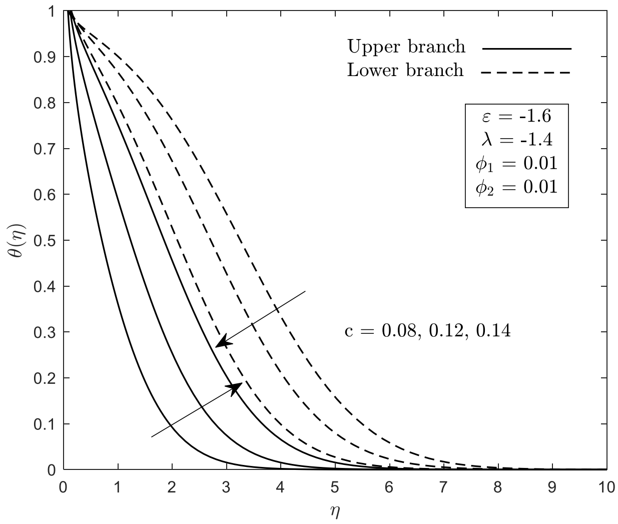

Fig. 11. Variation of c on dimensionless temperature profiles $\theta(\eta)$

Table 5
Minimum eigenvalues γ when $\mathrm{Pr}=6.2$, $c=0.1$ and $\varepsilon=-1.0$ for different values of λ, ϕ_1 and ϕ_2

$\boldsymbol{\phi_1}$ and $\boldsymbol{\phi_2}$	λ	Upper branch solution	Lower branch solution
$\boldsymbol{\phi_1 = \phi_2 = 0}$	-1.93	0.0675	-0.0625
	-1.935	0.0646	-0.0600
	-1.9358	0.0641	-0.0596
$\boldsymbol{\phi_1 = 0.01, \phi_2 = 0}$	-2.02	0.0597	-0.0558
	-2.024	0.0571	-0.0536
	-2.0248	0.0566	-0.0531
$\boldsymbol{\phi_1 = \phi_2 = 0.01}$	-2.11	0.0717	-0.0661
	-2.113	0.0702	-0.0648
	-2.1136	0.0699	-0.0645

7. Conclusions

The consideration of hybrid nanofluid in the steady flow of a moving thin needle with the presence of the buoyancy effect has been performed in this work. The followings are the effect of the physical parameters of interest on the characteristics of the fluid flow:

i. Hybrid nanofluid gives higher magnitudes of the reduced skin friction coefficient and local Nusselt number than nanofluid and water.
ii. The presence of high copper nanoparticle volume fraction ϕ_2 increases the reduced skin friction and local Nusselt number when ϕ_1 is constant.
iii. The existence of the dual solutions is found when the needle opposes the free-stream direction ($\varepsilon < 0$) and when the flow is opposing ($\lambda < 0$).
iv. The skin friction coefficient and the rate of heat transfer occur between the needle and fluid flow increases when the needle wall becomes thinner.
v. It has been proved by stability analysis that the lower branch solution represents an unstable solution, while the upper branch solution represents a stable solution.

Acknowledgement
The authors would like to acknowledge the financial support received from Universiti Putra Malaysia through Putra Grant (GP-IPS/2018/9667900) and from Ministry of Higher Education Malaysia through Fundamental Research Grant Scheme (FRGS/1/2018/STG06/UPM/02/4/55401 55).

References

[1] Choi, S.U.S. "Enhancing thermal conductivity of fluids with nanoparticles." In *Proceedings of the ASME International Mechanical Engineering Congress and Exposition* 231, (1995): 99-105.
[2] Rana, Puneet, and R. Bhargava. "Flow and heat transfer of a nanofluid over a nonlinearly stretching sheet: a numerical study." *Communications in Nonlinear Science and Numerical Simulation* 17, no. 1 (2012): 212-226.
[3] Bachok, Norfifah, Anuar Ishak, Roslinda Nazar, and Norazak Senu. "Stagnation-point flow over a permeable stretching/shrinking sheet in a copper-water nanofluid." *Boundary Value Problems* 2013, no. 1 (2013): 39.
[4] Salleh, Siti Nur Alwani, Norfifah Bachok, and Norihan Md Arifin. "Rotating Flow Over A Permeable Shrinking Surface in A Nanofluid." *Asian Journal of Mathematics and Computer Research* (2016): 290-305.
[5] Japar, Wan Mohd Arif Aziz, Nor Azwadi Che Sidik, Siti Rahmah Aid, Yutaka Asako, and Tan Lit Ken. "A Comprehensive Review on Numerical and Experimental Study of Nanofluid Performance in Microchannel Heatsink (MCHS)." *Journal of Advanced Research in Fluid Mechanics and Thermal Sciences* 45, no. 1 (2018): 165-176.
[6] Acharya, Nilankush, Kalidas Das, and Prabir Kumar Kundu. "Influence of multiple slips and chemical reaction on radiative MHD Williamson nanofluid flow in porous medium: A computational framework." *Multidiscipline Modeling in Materials and Structures* 15, no. 3 (2019): 630-658.
[7] Sarkar, Jahar, Pradyumna Ghosh, and Arjumand Adil. "A review on hybrid nanofluids: recent research, development and applications." *Renewable and Sustainable Energy Reviews* 43 (2015): 164-177.
[8] Suresh, S., K. P. Venkitaraj, P. Selvakumar, and M. Chandrasekar. "Synthesis of Al2O3–Cu/water hybrid nanofluids using two step method and its thermo physical properties." *Colloids and Surfaces A: Physicochemical and Engineering Aspects* 388, no. 1-3 (2011): 41-48.
[9] Nine, Md J., B. Munkhbayar, M. Sq Rahman, Hanshik Chung, and Hyomin Jeong. "Highly productive synthesis process of well dispersed Cu2O and Cu/Cu2O nanoparticles and its thermal characterization." *Materials Chemistry and Physics* 141, no. 2-3 (2013): 636-642.
[10] Madhesh, D., R. Parameshwaran, and S. Kalaiselvam. "Experimental investigation on convective heat transfer and rheological characteristics of Cu–TiO2 hybrid nanofluids." *Experimental Thermal and Fluid Science* 52 (2014): 104-115.
[11] Afrand, Masoud, Davood Toghraie, and Nima Sina. "Experimental study on thermal conductivity of water-based Fe3O4 nanofluid: development of a new correlation and modeled by artificial neural network." *International Communications in Heat and Mass Transfer* 75 (2016): 262-269.
[12] Esfe, Mohammad Hemmat, Ali Alirezaie, and Mousa Rejvani. "An applicable study on the thermal conductivity of SWCNT-MgO hybrid nanofluid and price-performance analysis for energy management." *Applied Thermal Engineering* 111 (2017): 1202-1210.
[13] Moghadassi, Abdolreza, Ehsan Ghomi, and Fahime Parvizian. "A numerical study of water based Al2O3 and Al2O3–Cu hybrid nanofluid effect on forced convective heat transfer." *International Journal of Thermal Sciences* 92 (2015): 50-57.
[14] Devi, S. Suriya Uma, and SP Anjali Devi. "Numerical investigation of three-dimensional hybrid Cu–Al2O3/water nanofluid flow over a stretching sheet with effecting Lorentz force subject to Newtonian heating." *Canadian Journal of Physics* 94, no. 5 (2016): 490-496.
[15] Mehryan, Seyed AM, Farshad M. Kashkooli, Mohammad Ghalambaz, and Ali J. Chamkha. "Free convection of hybrid Al2O3-Cu water nanofluid in a differentially heated porous cavity." *Advanced Powder Technology* 28, no. 9 (2017): 2295-2305.
[16] Ashorynejad, Hamid Reza, and Alireza Shahriari. "MHD natural convection of hybrid nanofluid in an open wavy cavity." *Results in Physics* 9 (2018): 440-455.
[17] Mansour, M. A., Sadia Siddiqa, Rama Subba Reddy Gorla, and A. M. Rashad. "Effects of heat source and sink on entropy generation and MHD natural convection of Al2O3-Cu/water hybrid nanofluid filled with square porous cavity." *Thermal Science and Engineering Progress* 6 (2018): 57-71.
[18] Acharya, Nilankush, Suprakash Maity, and Prabir Kumar Kundu. "Influence of inclined magnetic field on the flow of condensed nanomaterial over a slippery surface: the hybrid visualization." *Applied Nanoscience* (2019): 1-15.
[19] Acharya, Nilankush, Raju Bag, and Prabir Kumar Kundu. "Influence of Hall current on radiative nanofluid flow over a spinning disk: a hybrid approach." *Physica E: Low-dimensional Systems and Nanostructures* 111 (2019): 103-112.

[20] Acharya, Nilankush, Suprakash Maity, and Prabir Kumar Kundu. "Framing the hydrothermal features of magnetized TiO2–CoFe2O4 water-based steady hybrid nanofluid flow over a radiative revolving disk." *Multidiscipline Modeling in Materials and Structures* (2019): 1-26.
[21] Waini, Iskandar, Anuar Ishak, and Ioan Pop. "Unsteady flow and heat transfer past a stretching/shrinking sheet in a hybrid nanofluid." *International Journal of Heat and Mass Transfer* 136 (2019): 288-297.
[22] Sheikholeslami, M., S. A. M. Mehryan, Ahmad Shafee, and Mikhail A. Sheremet. "Variable magnetic forces impact on magnetizable hybrid nanofluid heat transfer through a circular cavity." *Journal of Molecular Liquids* 277 (2019): 388-396.
[23] Acharya, Nilankush. "On the flow patterns and thermal behaviour of hybrid nanofluid flow inside a microchannel in presence of radiative solar energy." *Journal of Thermal Analysis and Calorimetry* (2019): 1-18.
[24] Acharya, Nilankush, Kalidas Das, and Prabir Kumar Kundu. "Effects of aggregation kinetics on nanoscale colloidal solution inside a rotating channel." *Journal of Thermal Analysis and Calorimetry* (2019): 1-17.
[25] Acharya, Nilankush, Raju Bag, and Prabir Kumar Kundu. "On the impact of nonlinear thermal radiation on magnetized hybrid condensed nanofluid flow over a permeable texture." *Applied Nanoscience* (2019): 1-13.
[26] Lee, Lawrence L. "Boundary layer over a thin needle." *The physics of fluids* 10, no. 4 (1967): 820-822.
[27] Narain, Jai Prakash, and Mahinder S. Uberoi. "Forced heat transfer over thin needles." *Journal of Heat Transfer* 94, no. 2 (1972): 240-242.
[28] Narain, Jai Prakash, and Mahinder S. Uberoi. "Combined forced and free-convection over thin needles." *International Journal of Heat and Mass Transfer* 16, no. 8 (1973): 1505-1512.
[29] Chen, J. L. S., and T. N. Smith. "Forced convection heat transfer from nonisothermal thin needles." *Journal of Heat Transfer* 100, no. 2 (1978): 358-362.
[30] Ishak, Anuar, Roslinda Nazar, and Ioan Pop. "Boundary layer flow over a continuously moving thin needle in a parallel free stream." *Chinese Physics Letters* 24, no. 10 (2007): 2895.
[31] Ahmad, Syakila, Norihan M. Arifin, Roslinda Nazar, and Ioan Pop. "Mixed convection boundary layer flow along vertical thin needles: Assisting and opposing flows." *International Communications in Heat and Mass Transfer* 35, no. 2 (2008): 157-162.
[32] Afridi, Muhammad Idrees, and Muhammad Qasim. "Entropy generation and heat transfer in boundary layer flow over a thin needle moving in a parallel stream in the presence of nonlinear Rosseland radiation." *International Journal of Thermal Sciences* 123 (2018): 117-128.
[33] Grosan, T., and I. Pop. "Forced convection boundary layer flow past nonisothermal thin needles in nanofluids." *Journal of Heat Transfer* 133, no. 5 (2011): 054503.
[34] Hayat, T., M. Ijaz Khan, M. Farooq, T. Yasmeen, and A. Alsaedi. "Water-carbon nanofluid flow with variable heat flux by a thin needle." *Journal of Molecular Liquids* 224 (2016): 786-791.
[35] Ahmad, Rida, M. Mustafa, and S. Hina. "Buongiorno's model for fluid flow around a moving thin needle in a flowing nanofluid: A numerical study." *Chinese journal of physics* 55, no. 4 (2017): 1264-1274.
[36] Soid, Siti Khuzaimah, Anuar Ishak, and Ioan Pop. "Boundary layer flow past a continuously moving thin needle in a nanofluid." *Applied Thermal Engineering* 114 (2017): 58-64.
[37] Salleh, Siti, Norfifah Bachok, Norihan Arifin, Fadzilah Ali, and Ioan Pop. "Magnetohydrodynamics flow past a moving vertical thin needle in a nanofluid with stability analysis." *Energies* 11, no. 12 (2018): 3297.
[38] Salleh, Siti Nur Alwani, Norfifah Bachok, Norihan Md Arifin, and Fadzilah Md Ali. "Slip Effect on Mixed Convection Flow Past a Thin Needle in Nanofluid Using Buongiorno's Model." *Journal of Advanced Research in Fluid Mechanics and Thermal Sciences* 59, no. 2 (2019) 243-253.
[39] Salleh, Siti Nur Alwani, Norfifah Bachok, Norihan Md Arifin, and Fadzilah Md Ali. "Numerical Analysis of Boundary Layer Flow Adjacent to a Thin Needle in Nanofluid with the Presence of Heat Source and Chemical Reaction." *Symmetry* 11, no. 4 (2019): 543.
[40] Merkin, J. H. "On dual solutions occurring in mixed convection in a porous medium." *Journal of engineering Mathematics* 20, no. 2 (1986): 171-179.
[41] Abu Bakar, Shahirah, Norihan Arifin, Fadzilah Md Ali, Norfifah Bachok, Roslinda Nazar, and Ioan Pop. "A stability analysis on mixed convection boundary layer flow along a permeable vertical cylinder in a porous medium filled with a nanofluid and thermal radiation." *Applied Sciences* 8, no. 4 (2018): 483.
[42] Salleh, Siti Nur Alwani, Norfifah Bachok, Norihan Md Arifin, and Fadzilah Md Ali. "Stability analysis of nanofluid flow past a moving thin needle subject to convective surface boundary conditions." In *AIP Conference Proceedings*, vol. 2184, no. 1, p. 060015. AIP Publishing LLC, 2019.
[43] Waini, Iskandar, Anuar Ishak, and Ioan Pop. "On the stability of the flow and heat transfer over a moving thin needle with prescribed surface heat flux." *Chinese Journal of Physics* 60, (2019): 651-658.
[44] Weidman, P. D., D. G. Kubitschek, and A. M. J. Davis. "The effect of transpiration on self-similar boundary layer flow over moving surfaces." *International journal of engineering science* 44, no. 11-12 (2006): 730-737.

[45] Oztop, Hakan F., and Eiyad Abu-Nada. "Numerical study of natural convection in partially heated rectangular enclosures filled with nanofluids." *International journal of heat and fluid flow* 29, no. 5 (2008): 1326-1336.
[46] Harris, S. D., D. B. Ingham, and I. Pop. "Mixed convection boundary-layer flow near the stagnation point on a vertical surface in a porous medium: Brinkman model with slip." *Transport in Porous Media* 77, no. 2 (2009): 267-285.
[47] Kumar, Sanjay, Pramod Kumar Sharma, and Puneet Rana. "Critical values in transport phenomena for curved power-law sheet utilizing Al2O3-Cu/water hybrid nanoliquid: Model prediction and stability analysis." *Advanced Powder Technology* 30, no. 11 (2019): 2787-2800.